

P1.4 THE UTILITY OF MESOSCALE VERSUS SYNOPTIC SCALE SURFACE OBSERVATIONS DURING THE LAHOMA HAIL AND WINDSTORM OF 17 AUGUST 1994

Dale A. Morris¹ and Paul R. Janish²

¹Oklahoma Climatological Survey, University of Oklahoma, Norman Oklahoma

²NSSL/MRAD/MAG, Norman, Oklahoma

1. INTRODUCTION

During the late evening hours of 16 August 1994, a mesoscale convective system (MCS) moved from central Nebraska into central Kansas where it began to weaken. Although the convection was expected to weaken (Janish *et al.* 1996) before moving into Oklahoma, redevelopment of the system occurred as it approached the Kansas/Oklahoma border around 1700 UTC on 17 August. The storm evolved into an unusually strong HP supercell, producing extreme wind and hail damage in Major, Garfield, Kingfisher, and Canadian counties in Oklahoma.

The Oklahoma Mesonet (Mesonet; Brock *et al.* 1995), an automated surface meteorological observing network with an average station spacing of about 33 km, recorded wind gusts of up to 50.7 m/s at its station located at Lahoma in north-central Oklahoma (Fig. 1) as the storm passed very near to the site. In addition, local residents reported large hail (one chunk measured 10 x 15 cm) that accumulated to depths of between 8 and 20 cm.

The storm also formed a mesocyclone a few miles southeast of Lahoma (Lemon and Parker 1996; Morris and Shafer 1996) as it moved southward into Kingfisher County, where a weak (F1) tornado was reported. Additional severe thunderstorms formed along the storm's outflow boundary in western Oklahoma, and eventually, the main storm evolved further into an MCS and moved into north Texas.

This paper presents an evaluation of surface observations from both the Mesonet and the Federal surface network during this event. Composites made from objectively derived parameters from both networks are compared with reflectivity measurements and vertically integrated liquid (VIL) calculations from the WSR-88D radar located at Twin Lakes.

2. METHODOLOGY

Corresponding author address: Dale A. Morris, Oklahoma Climatological Survey, 100 E. Boyd, Suite 1210, Norman, OK 73019; e-mail: dmorris@uoknor.edu.

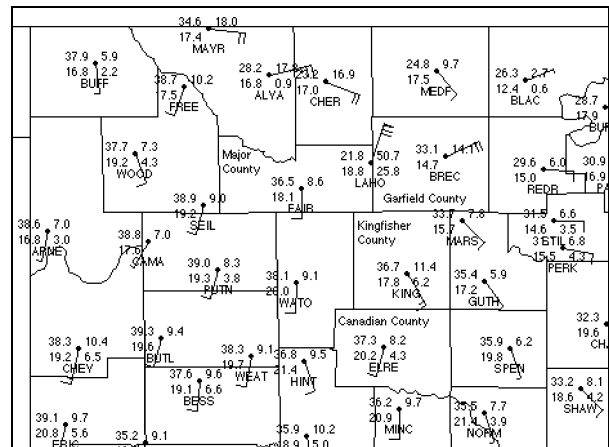


Figure 1. Oklahoma Mesonet observations at 1950 UTC on 17 August 1994. Station model plot is as follows: upper left: air temperature (°C); lower left: dew point (°C); upper right: peak wind gust at 10 m (m/s); lower right: wind speed at 2 m (m/s). Wind barbs drawn so that a flag represents 25 m/s; a full barb represents 5 m/s and a half barb represents 2.5 m/s. Mesonet site ID's are indicated and county names are shown for counties referenced in the text.

2.1 Objective Analysis

A four-pass Barnes (1994a,b) scheme was employed to analyze observations and derived parameters from both networks. Figure 2 shows the two nested grids that were established, each with 12 km grid spacing. Mesonet data were analyzed to the inner ("mesoscale") grid, while the outer ("synoptic") grid that extended well beyond the borders of Oklahoma was used for the SAO data. As suggested by Barnes (1994a), all available observations were used in each analysis, and the weighting functions were tuned according to the station spacing. The median nearest-neighbor spacing of the Mesonet stations was approximately 33 km, while the same calculation for the SAO network resulted in a median spacing of 37 km. The latter spacing was lower than expected because of the clustering effect of Federal stations located in metropolitan areas. Therefore, a "super-obbing" approach was used to decluster the SAO

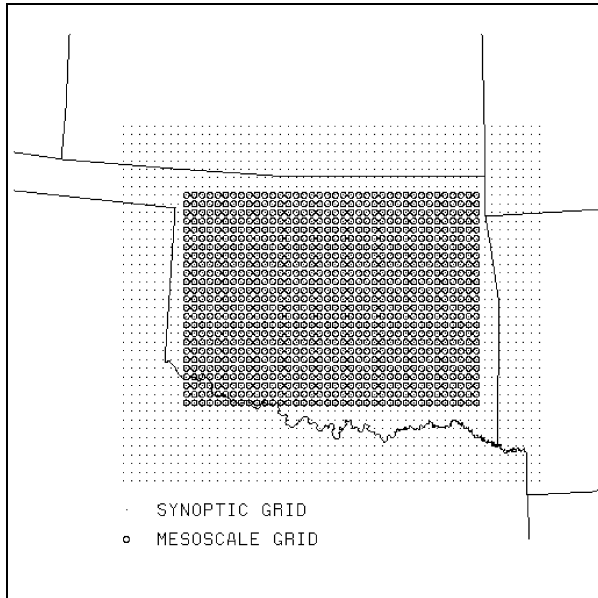


Figure 2. The objective analysis grids and domains. Mesonet data were analyzed to the "mesoscale" grid, and the Federal data were analyzed to the "synoptic" grid.

data, producing a revised station spacing of about 78 km. Even with these considerations, this work did not attempt to calculate the "best" analysis possible from each network. Rather, the intent was to compute analyses that were adequate to permit fair comparisons of derived products from both networks.

Even though Mesonet data has five-minute time resolution, the mesoscale analysis was performed at fifteen-minute intervals from 1500 UTC on 17 August through 0300 UTC on 18 August because Mesonet data are available operationally every fifteen minutes. The following parameters *measured* by the Mesonet were analyzed: air temperature (TAIR), wind, 10-cm soil temperatures under natural sod and under bare soil (TS10 and TB10, respectively) and solar radiation (SRAD). Additionally, the following *derived* parameters were computed and analyzed: dew point (TDEW), altimeter setting (PALT), mass divergence (DVRG), moisture convergence (MCNV), and lifted index (LIFT). The temperature, dew point, mean sea-level pressure, and wind fields from the SAO network were analyzed at hourly intervals. Similar derived quantities from the SAO data also were calculated over the same time period as the Mesonet analysis.

The lifted index analysis for both networks utilized all available NWS soundings from Amarillo, Dodge City, Fort Worth, Longview, Little Rock, Midland, Norman, Topeka, and Monett plus special soundings taken at Lamont, Oklahoma, by the Atmospheric Radiation Measurement (ARM; Stokes and Schwartz 1994) program. A Barnes-type weighting function was

used to interpolate 500 mb temperatures from each sounding to fifteen-minute or hourly intervals. Fifteen-minute mesoscale and hourly synoptic grids of 500 mb temperature were then produced using the four-pass Barnes scheme in space. Surface lifted parcel temperatures at 500 mb were calculated from each network, and finally a lifted index was computed for each grid point.

2.2 Radar Analysis

Level II data from the Twin Lakes WSR-88D radar (KTLX) were used as the verification field in this study. Every volume scan recorded between 1800 UTC on 17 August and 0400 UTC on 18 August was utilized. For the lowest elevation angle and for every grid cell shown in Figure 2, the maximum reflectivity values from the range bins located in the grid cell were assigned to that grid cell for both analysis grids. In addition, VIL values were obtained using the operational VIL/Echo Top algorithm provided by the WSR-88D Operational Support Facility. Using an approach similar to the transformation of the reflectivity data, the maximum VIL values were assigned to both analysis grids.

2.3 Composite Analysis

To perform the comparisons that are the subject of this work, and in order to better understand the meteorological signal present in the observations from both surface networks, a composite analysis was produced. This type of analysis has been applied previously to upper-air analyses for MCS events (Fritsch and Maddox 1981) and to heavy rain events (Grice and Maddox 1982). More recently, Junker *et al.* (1995) used a similar technique in evaluating several forecast rules as applied to the Great Midwest Flood of 1993.

In the present case, the analysis methodology described in Sections 2.1 and 2.2 produced surface observations, radar reflectivities, and VIL values *on the same grid* for both the synoptic and mesoscale data sets. From the 95 volume scans that were available, the grid points with the maximum VIL were identified for both the synoptic and mesoscale grids. Occasionally the maximum VIL was associated with the storms in far western Oklahoma that formed along the Lahoma storm's outflow boundary, requiring the centroid of the Lahoma storm to be located subjectively. This objective/subjective process yielded 57 and 69 mesoscale and synoptic centroids, respectively. More synoptic centroids resulted because the synoptic domain is larger than the mesoscale domain.

A movable 21 by 21 subgrid, with a 12 km mesh, was centered on each storm centroid. Composite maps of the VIL, reflectivity, and surface gridded parameters from

both networks were produced relative to the storm centroid. The various subgrids containing surface data relative to the storm centroid were chosen by minimizing the time difference between the VIL centroids and the various surface parameter grids. Composites were determined by a simple arithmetic average over all available subgrids (thus, over time).

3. RESULTS

The methodology described in Section 2 when applied to the Lahoma storm event yielded 22 and 8 Mesonet and SAO subgrids, respectively for each parameter. The resulting composite pictures, or arithmetic time averages, of several parameters are described below. Each plot contains the composite VIL and wind field for the event. The "synoptic" and "mesoscale" VIL fields appear slightly different, because the larger synoptic domain produced more synoptic VIL centroids than the mesoscale domain.

3.1 Air Temperature

Figure 3 shows the composite Mesonet and SAO air temperature maps. Both the Mesonet and SAO temperature fields contain a cold pool north of the storm. The Mesonet cold pool is more intense (the minimum Mesonet composite grid point temperature is 21.9 °C) than the SAO cold pool (minimum grid point temperature is 24.7 °C), and is located closer to the storm. The temperature gradient on the Mesonet plot is also much stronger (approximately 0.2 °C/km versus 0.08 °C/km).

A strong line of confluence is apparent in the wind field in Fig. 3a along the leading edge of the temperature gradient with easterly flow to the northeast of the storm. Fig. 3b indicates some confluence as well, but the signature is not as strong. The pattern in Fig. 3a is

reminiscent of a synoptic-scale front where a field of deformation acts to tighten a temperature gradient. Additionally, Figure 3a indicates the average position of the mesohigh relative to the storm through the divergent wind field located to the east of the storm centroid.

3.2 Dew Point

The Mesonet dew point field (Fig. 4a) is a relatively flat field over the domain. The SAO dew point field (Fig. 4b) is also relatively uniform, but approximately 1-2 °C lower than the Mesonet dew points. This finding is consistent with the fact that Crawford *et al* (1995) found Mesonet dew points to be 1-2 °C higher at two sites co-located with ASOS (Automated Surface Observing System) units. Factors related to the differences in dew points between the two networks include: (a) the Mesonet measures relative humidity and the Federal network directly measures dew point and (b) the SAO sites tend to be located near airports, but Mesonet stations are typically located in rural pasture areas. At any rate, Figure 4 shows the predominate southerly flow advecting higher dew points into the storm complex.

3.3 Altimeter Setting

The ridge in the composite altimeter setting field from the Mesonet (Fig 5a) agrees with the position of the mesohigh as revealed by the wind field. The low in the northwest corner of the domain likely is induced by warm temperatures (compare with Fig. 3a). The SAO composite pressure gradient (Fig. 5b) is weaker than the Mesonet composite. This is also in agreement with the wind field. The maximum SAO composite wind speed is 5.5 m/s and the maximum Mesonet composite wind speed is 10.3 m/s.

3.4 Divergence

Figure 6 depicts the mass divergence fields from the Mesonet and SAO composites. The prominent feature in both fields is a convergence/divergence couplet

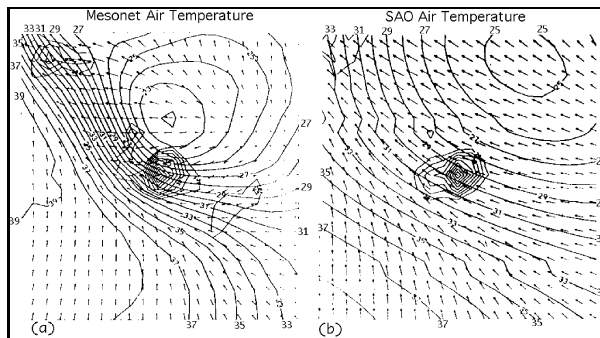


Figure 3. Composite air temperature (dark contours), VIL (light contours), and wind vector fields (arrows) for (a) the Mesonet and (b) the SAO network. Temperature contour interval is 1 °C and the VIL contour interval is 10 kg/m².

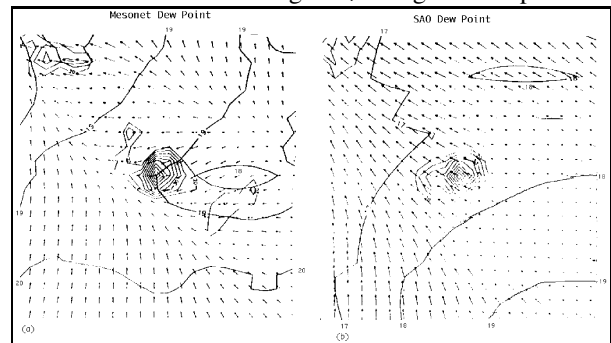


Figure 4. Same as in Fig. 3 except for dew point (contour interval is 1 °C).

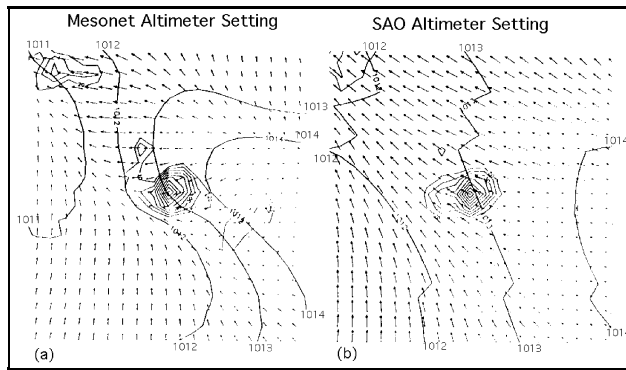


Figure 5. Same as in Fig. 3 but for altimeter setting (contour interval is 1 mb).

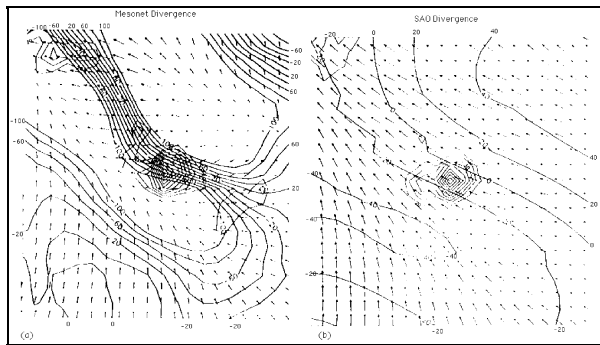


Figure 6. Same as in Fig. 3 except divergence is analyzed (contour interval is $20 \times 10^{-3} \text{ s}^{-1}$). The Mesonet values range from -225×10^{-3} to $+223 \times 10^{-3} \text{ s}^{-1}$ and the SAO values range from -42×10^{-3} to $+51 \times 10^{-3} \text{ s}^{-1}$.

oriented northeast-southwest (i.e. perpendicular to the line of confluence). The magnitude of the divergence in the Mesonet plot is much stronger than the SAO divergence. As expected, the center of convergence is oriented along the line of confluence in the Mesonet plot, and the maximum divergence is located near the mesohigh. Finally, the center of the area of divergence in the SAO composite is located much farther northeast of the storm than the divergence maximum in the Mesonet case.

3.5 Moisture Convergence

A couplet of moisture convergence and moisture divergence is evident on the Mesonet moisture convergence composite (Fig. 7a). The line connecting the centers of the couplet is oriented almost north-south. The same general features are apparent in the SAO composite (Fig 7b), but the line through the centers of the couplet is oriented northeast-southwest. As in the case of mass divergence, the magnitude of the convergence in the SAO composite is weaker than the Mesonet composite.

3.6 Lifted Index

The Mesonet and SAO lifted index composites are given in Fig. 8a and Fig. 8b, respectively. The Mesonet lifted index plot resembles the temperature composite in Fig. 3a. This is expected because the 500 mb temperatures do not change appreciably over a domain 252 km on a side. The SAO composite appears to have less instability than the Mesonet composite (minimum SAO lifted index of approximately -3.6° C compared to -6.3° C for the Mesonet). The $1\text{-}2^\circ \text{ C}$ dew point bias described in Section 3.2 could be responsible for the differences in the magnitudes of lifted index. Finally, the Mesonet composite indicates a region of stability associated with the cold pool and mesohigh. This stable area does not appear on the SAO composite.

3.7 Soil Temperature

Figure 9 shows the Mesonet composite of soil temperature at a depth of 10 cm under bare soil. Clearly, the footprint of the storm can be seen in the minimum

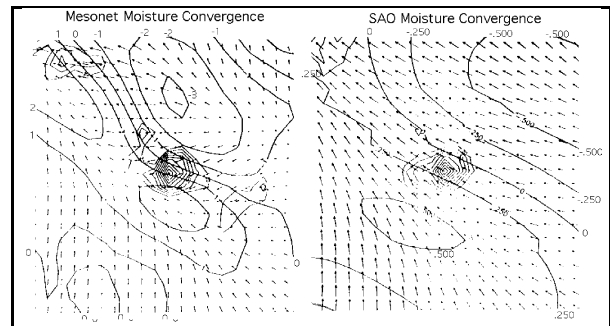


Figure 7. Same as in Fig. 3 but for moisture convergence. Mesonet contour interval is $1 \text{ g}/(\text{kg} \text{ s})$ and the SAO contour interval is $0.25 \text{ g}/(\text{kg} \text{ s})$.

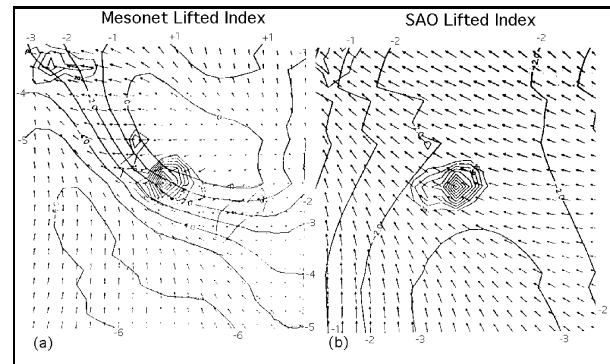


Figure 8. Same as in Fig. 3 except for lifted index. Contour interval is 1° C .

located northeast of the storm. Animated loops of the Barnes analysis of the soil temperatures reveal about a one-hour lag between the cooling at 1.5 m above the surface and 10 cm below the surface. A similar composite of the soil temperature under natural sod contains a similar pattern except the amplitude is weaker (not shown). However, the animated loops of the soil temperatures under sod do not show a pronounced footprint as the bare soil temperatures do.

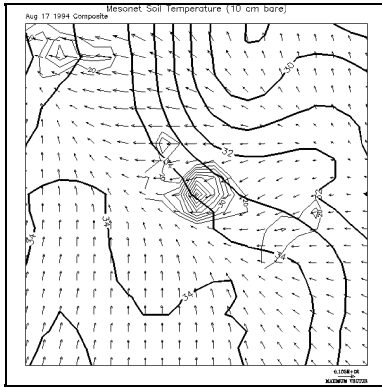


Figure 9. Mesonet composite plot of soil temperature under bare soil at a depth of 10 cm. Contour interval is 1° C).

4. DISCUSSION

The composite plots presented in this study reveal qualitatively that there is more detail in the meteorological signal in the Mesonet observations than in the SAO observations for the Lahoma case. Ongoing research is attempting to quantify the improvements in the level of detail in the Mesonet composites, to apply the methodology to other types of events (e.g. MCS and tornadic supercell events), and to investigate the predictive value of the Mesonet observations.

One factor that enters into this analysis is the spatial sampling properties of the two networks. These composites represent the average conditions relative to the storm. At any given time, each network could reveal patterns different from those presented here. The individual analyses from the Mesonet closely resemble the composite picture, but the SAO analyses occasionally differ from the composite. For example, the SAO divergence analysis shows amplitude comparable to the Mesonet analysis when the storm is close to SAO sites (e.g. END and OKC), but the amplitude is weaker when the storm is between observing sites. This "aliasing" phenomenon is present in Mesonet observations as well. One reason for the notoriety of the Lahoma storm is the Mesonet observations of 50.7 m/s wind gusts. Other reports of strong winds (46 m/s) from storms in western Oklahoma that formed along the outflow boundary were received, but the high winds did not directly affect a Mesonet site.

This type of analysis is helpful in validating the

current conceptual models of the interactions of convective storms with their environment. In addition, composites of Mesonet observations are useful in understanding the convective initiation problem and should provide the basis of comparing new mesoscale and stormscale numerical models with real world observations.

5. ACKNOWLEDGEMENTS

The SAO data analyzed in this paper was provided by Jim Henderson from the Aviation Weather Center of the National Centers for Environmental Prediction. The entire Mesonet staff deserves credit for keeping the network operational. The WSR-88D Operational Support Facility provided the VIL algorithm, and the KTLX data was provided by Larry Ruthi from the Norman NWS office. Finally, constructive criticism was provided by Don Burgess, Les Lemon, and Ken Crawford.

6. REFERENCES

- Barnes, S.L., 1994a: Application of the Barnes objective analysis scheme. Part I: Effects of undersampling, wave position, and station randomness. *J. Atmos. Oceanic Technology*, **11**, 1433-1448.
- Barnes, S.L., 1994b: Application of the Barnes objective analysis scheme. Part III: Tuning for minimum error. *J. Atmos. Oceanic Technology*, **11**, 1459-1479.
- Brock, F.V., K.C. Crawford, R.L. Elliott, G.W. Cuperus, S.J. Stadler, Johnson, and M.D. Eilts, 1995: The Oklahoma Mesonet: a technical overview. *J. Atmos. Oceanic Technology*, **12**, 5-19.
- Crawford, K.C., D.S. Arndt, D.J. Shellberg, and B.M. Brus, 1995: A comparison of differences in meteorological measurements made by the Oklahoma Mesonet at two co-located ASOS sites. *11th Intl. Conf. on Inter. Info. and Proc. Sys.*, Amer. Meteor. Soc., 299-303.
- Fritsch, J.M., and R.A. Maddox, 1981: Convectively driven mesoscale weather systems aloft. Part I: Observations. *J. Appl. Met.*, **20**, 9-19.
- Grice, G.K., and R.A. Maddox, 1982: Synoptic aspects of heavy rain events in south Texas associated with the westerlies. NOAA Technical Memorandum NWS SR-106, Fort Worth Texas.
- Janish, P.R., R.H. Johns, and K.C. Crawford, 1996: An evaluation of the 17 August 1994 Lahoma supercell/MCS event using conventional and non-conventional forecasting techniques. *18th Conf. on Severe Local Storms*, Amer. Meteor. Soc.
- Junker, 1993: Meteorological conditions associated with the Great Midwest Flood of 1993. *Preprints, 14th Conf. on Weather Analysis and Forecasting*, Amer. Meteor. Soc.
- Lemon, L.R. and S. Parker, 1996: The Lahoma storm deep convergence zone: its characteristics and role in storm dynamics and severity. *18th Conf. on Severe Local Storms*, Amer. Meteor. Soc.
- Morris, D.A., and M.A. Shafer, 1996: Detailed surface observations during the Lahoma hail and windstorm. *18th Conf. on Severe Local Storms*, Amer. Meteor. Soc.
- Stokes, G.M., and S.E. Schwartz, 1994: The Atmospheric Radiation Measurement (ARM) Program: Programmatic background and design of the Cloud and Radiation Test Bed. *Bull. Amer. Meteor. Soc.*, **75**, 1201-1221.